

Role of degeneracy, hybridization, and nesting in the properties of multiorbital systemsAndrew Nicholson,^{1,2} Qinlong Luo,^{1,2} Weihao Ge,^{1,2} José Riera,³ Maria Daghofer,⁴ George B. Martins,⁵ Adriana Moreo,^{1,2} and Elbio Dagotto^{1,2}¹*Department of Physics and Astronomy, The University of Tennessee, Knoxville, Tennessee 37996, USA*²*Materials Science and Technology Division, Oak Ridge National Laboratory, Oak Ridge, Tennessee 32831, USA*³*Instituto de Física Rosario, Universidad Nacional de Rosario, 2000-Rosario, Argentina*⁴*IFW Dresden, P. O. Box 27 01 16, D-01171 Dresden, Germany*⁵*Department of Physics, Oakland University, Rochester, Michigan 48309, USA*

(Received 14 July 2011; published 20 September 2011)

To understand the role that degeneracy, hybridization, and nesting play in the magnetic and pairing properties of multiorbital Hubbard models we here study numerically two types of two-orbital models, both with holelike and electron-like Fermi surfaces (FS's) that are related by nesting vectors $(\pi, 0)$ and $(0, \pi)$. In one case the bands that determine the FS's arise from strongly hybridized degenerate d_{xz} and d_{yz} orbitals, while in the other the two bands are determined by nondegenerate and nonhybridized s -like orbitals. Using a variety of techniques, in the weak-coupling regime it is shown that only the model with hybridized bands develops metallic magnetic order, while the other model exhibits an ordered excitonic orbital-transverse spin state that is insulating and does not have a local magnetization. However, both models display similar insulating magnetic stripe ordering in the strong-coupling limit. These results indicate that nesting is a necessary but not sufficient condition for the development of ordered states with finite local magnetization in multiorbital Hubbard systems; the additional ingredient appears to be that the nested portions of the bands need to have the same orbital flavor. This condition can be achieved via strong hybridization of the orbitals in weak coupling or via the FS reconstruction induced by the Coulomb interactions in the strong-coupling regime. This effect also affects the pairing symmetry as demonstrated by the study of the dominant pairing channels for the two models.

DOI: [10.1103/PhysRevB.84.094519](https://doi.org/10.1103/PhysRevB.84.094519)

PACS number(s): 74.20.Rp, 71.10.Fd, 74.70.Xa, 75.10.Lp

I. INTRODUCTION

Among the several aspects of the study of the iron-based superconductors that are still controversial and unsettled,¹ the following two questions have attracted considerable attention: (i) Does the magnetic order observed in the parent compounds² arise from the nesting properties of the noninteracting (or high temperature) Fermi surface^{3,4} or should a better description be based on the superexchange Heisenberg interactions between localized magnetic moments?⁵ and (ii) what is the pairing mechanism, to what extent is the pairing symmetry determined by nesting, and what is the actual symmetry and momentum dependence of the pairing operator? In particular, what is the role that the orbital degrees of freedom play in this context?

The origin of the magnetic state is being vigorously debated. One proposal, based on fermiology, is the excitonic mechanism in which electron-hole pairs are formed by one electron and one hole from different FS's nested with nesting vector \mathbf{Q} . In this context some studies disregard the orbital structure of the bands^{3,6-8} while others stress the role played by their orbital composition.⁹⁻¹⁵ Another approach focuses on the order of the localized moments that develop in the presence of strong Coulomb interactions^{5,16-18} and relies on *ab initio* results^{19,20} that suggest that the pnictides are moderately, rather than weakly, correlated, a conclusion supported by photoemission measurements indicating mass enhancements due to electron correlations as large as 2–3.²¹

The pairing mechanism in the pnictides is also controversial. Most of the pairing operators that have been proposed in the literature either ignore the multiorbital characteristics of the problem or consider Cooper pairs that are made from electrons located at the same orbital. A majority of these

previous studies have been performed in the weak-coupling limit. The original proposal of the s_{\pm} pairing state dealt with the overall symmetry of the pairing operator but without distinguishing among the spatial vs. orbital contributions to its particular form.^{3,4} Other authors²² have considered a spin-fluctuation-induced pairing interaction and also assumed that Cooper pairs are predominantly made of electrons in the same orbital. A random-phase approximation (RPA) analysis¹¹ concluded that the pairing is, again, intraorbital, both for the A_{1g} (s -wave) and B_{1g} (d -wave) symmetries. Among the authors that have used the conceptually different strong-coupling approach, some have studied effective single orbital models⁵ while others incorporated two orbitals²³ but still considered only intraorbital pairing operators. The same model was also studied under a mean-field approximation²⁴ with the assumption that exchange takes place between spins on the same orbitals and, again, only intraorbital pairs were proposed.

Among the early first studies of multiband superconductors, Suhl *et al.*²⁵ considered two tight-binding bands, hypothetically identified with s and d orbitals, and the effect of weak electron-phonon interactions. Under these assumptions, it was reasonable to expect that the Cooper pairs would be formed by electrons belonging to the same band. However, the actual orbital composition of the pairs was not addressed. The interacting portion of the Hamiltonian was written in the band representation and this model was proposed by analogy with models used in the Bardeen-Cooper-Schrieffer (BCS) theory, assuming that emission and absorption of a phonon could occur in four ways. These four processes corresponded to pair scattering within each of the two FS's and pair hopping from one FS to the other. This last process would occur if the

exchanged phonon has enough momentum to allow the Cooper pair to jump from an FS to the other, and it can occur even if the orbitals do not hybridize to form the bands.²⁶ In this case, the expected pairing operator is the traditional on-site s -wave state of the BCS theory, with a momentum-independent gap. In principle, independent gaps may arise on the different FS's²⁵ unless the orbitals are hybridized by the symmetries of the Hamiltonian, in which case the gaps will have to be related to each other and obey the symmetries of the system.¹²

The previous discussion applies to superconductors driven by the electron-phonon interaction. However, it is believed that the most relevant interactions in the pnictides are the Coulomb repulsion and Hund magnetic exchange. These interactions are more easily expressed in real space and in the orbital representation. In fact, the effective form of the Coulomb interaction in the band representation is more complicated than the expression provided by Suhl *et al.*²⁵ for the electron-phonon interaction. In particular, it has been shown⁶ that a pair-hopping term, such as the one introduced by Suhl *et al.*, occurs only if the orbitals get hybridized to form the bands. If the orbitals are *not* hybridized, this type of term is not present in the effective interaction Hamiltonian. In addition, when the bands are made of hybridized orbitals, as is the case for the iron pnictides,²⁷ the actual orbital structure of the pairs needs to be considered since, due to the Coulomb repulsion, on-site pairing is not expected to occur, and the overall symmetry properties of the pairing operators may be a function of their spatial and orbital components.^{10,12}

To understand the role that the orbitals play in the case of electrons with strongly hybridized bands that interact via the Coulomb repulsion, as believed to occur in the case of the pnictides in the context of the magnetic scenario for superconductivity, in this manuscript we present and discuss Lanczos numerical, real-space Hartree-Fock mean-field, and RPA studies of two different two-orbital models that both display identical Fermi surfaces. One of them is the well-known and widely used two-orbital model for the pnictides^{9,10,12} based on the two strongly hybridized degenerate d_{xz} and d_{yz} orbitals of iron, while the second is a two-band “toy model” (dubbed the s model) whose bands arise from two nonhybridized, nondegenerate, s -like orbitals. The latter model has an FS qualitatively similar to that of the pnictides. In both cases a hole (electron) FS is located at the Γ/M (X/Y) points of the Brillouin zone (BZ). The hole and electron FS's are connected by nesting vectors $(\pi, 0)$ and $(0, \pi)$. The role that the nesting and the orbitals play in the magnetic and pairing properties of these models will be investigated and discussed here, in both the weak- and strong-coupling regimes.

Besides its conceptual relevance, the results presented here should also be framed in the context of recent bulk-sensitive laser angle-resolved photoemission (ARPES) experiments²⁸ on $\text{BaFe}_2(\text{As}_{0.65}\text{P}_{0.35})_2$ and $\text{Ba}_{0.6}\text{K}_{0.4}\text{Fe}_2\text{As}_2$. The main conclusion of Ref. 28 is the existence of orbital-independent superconducting gaps that are not expected from spin fluctuations and nesting mechanisms but are claimed to be better explained by magnetism-induced interorbital pairing and/or orbital fluctuations. This is argued based on the observation that the $3z^2 - r^2$ orbital that forms one of the hole pockets at the BZ center, but that does not have a nested partner with the same orbital at the electron pockets, nevertheless

appears to develop a superconducting gap. Another interesting experimental result that challenges the role of nesting in the physics of the pnictides is a careful measurement of the de Haas-van Alphen (dHvA) effect in BaFe_2P_2 , the end member of the series $\text{BaFe}_2(\text{As}_{1-x}\text{P}_x)_2$, indicating that this nonmagnetic and nonsuperconducting compound displays the best nesting of all the compounds in the series.²⁹

The manuscript is organized as follows. In Sec. II the models are introduced. The magnetic properties are presented in Sec. III while the pairing properties are the subject of Sec. IV. Section V is devoted to the conclusions.

II. MODELS

A. d model

The reference model that will be considered here is the widely used two-orbital model^{9,10,12} based on the d_{xz} (x) and d_{yz} (y) Fe orbitals of the pnictides. Since the two orbitals are degenerate, an important detail is that the direction along which each orbital is defined is actually arbitrary. Two directions have been used in the literature: x, y ,^{9,10,12} with the x and y axes along the directions that connect nearest-neighbor iron atoms, and X, Y ,^{4,30} with the X and Y axis rotated 45° with respect to the (x, y) set. In terms of the d_{xz} and d_{yz} orbitals, the tight-binding dispersion of the two-orbital model is given by³¹

$$\begin{aligned} \xi_{xy}(\mathbf{k}) = & [-(t_1 + t_2)(\cos k_x + \cos k_y) \\ & - 4t_3 \cos k_x \cos k_y - \mu] \tau_0 \\ & - (t_1 - t_2)(\cos k_x - \cos k_y) \tau_3 \\ & - 4t_4 \sin k_x \sin k_y \tau_1, \end{aligned} \quad (1)$$

where τ_i , with $i = 1, 2, 3$, are the Pauli matrices and τ_0 is the 2×2 identity matrix. The τ_i matrices act in orbital space. Note that $\xi_{xy}(\mathbf{k})$ must transform as the A_{1g} representation of D_{4h} ; in this representation τ_0 transforms as A_{1g} , τ_1 as B_{2g} , and τ_3 as B_{1g} . However, if the degenerate d orbitals are expressed in terms of the (X, Y) axes as (d_X, d_Y) , then the tight-binding dispersion becomes:³⁰

$$\begin{aligned} \xi_{XY}(\mathbf{k}) = & [-(t_1 + t_2)(\cos k_x + \cos k_y) \\ & - 4t_3 \cos k_x \cos k_y - \mu] \tau_0 \\ & - (t_1 - t_2)(\cos k_x - \cos k_y) \tau_1 \\ & - 4t_4 \sin k_x \sin k_y \tau_3. \end{aligned} \quad (2)$$

Note that the XY basis is chosen just for the orbitals while in real space the system of coordinates is still given by (x, y) . $\xi_{XY}(\mathbf{k})$ also has to transform as A_{1g} which means that, when the orbitals are defined in the (X, Y) basis, then τ_1 transforms as B_{1g} and τ_3 as B_{2g} . It can be shown that since τ_1 is the matrix that indicates interorbital electron hopping, this kind of hopping happens between nearest-neighbors [next-nearest-neighbors] in the (X, Y) [(x, y)] representation.

As previously discussed, if the values of the parameters are set to $t_1 = -1$, $t_2 = 1.3$, $t_3 = t_4 = -0.85$, and $\mu = 1.54$ then the Fermi surface (shown in Fig. 1 together with the band dispersion) for the tight-binding Hamiltonian is in qualitative agreement with band structure calculations for the pnictides⁹ once folding to the reduced BZ is performed. Note that the

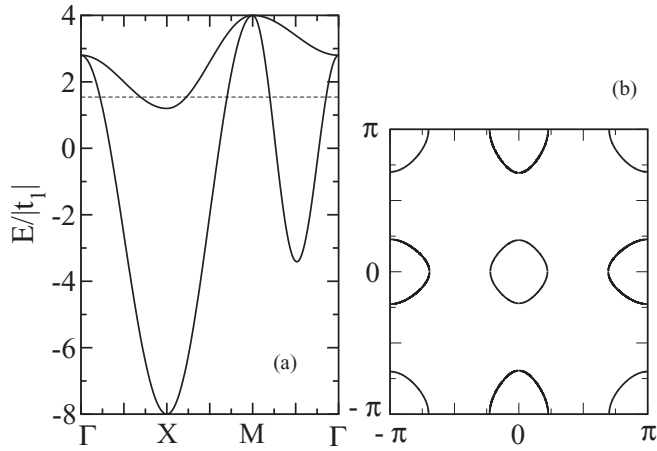


FIG. 1. (a) Band dispersion and (b) Fermi surface for the half-filled two-orbital d model for the pnictides, with the hopping parameters introduced in Ref. 9.

system is half filled (two electrons per Fe site on average) and, due to the orbital degeneracy, each orbital is half filled as well, despite the fact that the bands are not equally filled.

An important characteristic of the two degenerate d orbitals in this model is that, around the hole pockets, a spinor describing the mixture of orbitals rotates twice on encircling these FS's. The inversion and time-reversal symmetry of the twice-degenerate d bands ensures that at each \mathbf{k} point it is possible to choose real spinor wave functions that are confined to a plane. The spinor has vorticity ± 2 around the hole pockets while there is no vorticity around the electron pockets.³⁰ As pointed out in Ref. 30, this topological characterization of the hole and electron pockets is also a characteristic of all the more realistic models for the pnictides that include additional orbitals.

B. s model

Let us introduce now a two-orbital model with two nondegenerate nonhybridized s -like bands, called $s_1(1)$ and $s_2(2)$, with dispersion relations given by

$$\xi_{s_1}(\mathbf{k}) = 2t_1(\cos k_x + \cos k_y) + 4t_2 \cos k_x \cos k_y - \mu, \quad (3)$$

and

$$\xi_{s_2}(\mathbf{k}) = 2t_3(\cos k_x + \cos k_y) + 4t_4 \cos k_x \cos k_y - \mu + \Delta, \quad (4)$$

where μ is the chemical potential and Δ is the energy difference between the two bands. The dispersions can also be written in the basis (s_1, s_2) , i.e., $(1, 2)$, using the τ_i matrices as in the previous case:

$$\begin{aligned} \xi_S(\mathbf{k}) = & \left[(t_1 + t_3)(\cos k_x + \cos k_y) + 2(t_2 + t_4) \cos k_x \cos k_y \right. \\ & \left. - \mu + \frac{\Delta}{2} \right] \tau_0 + \left[(t_1 - t_3)(\cos k_x + \cos k_y) \right. \\ & \left. + 2(t_2 - t_4) \cos k_x \cos k_y - \frac{\Delta}{2} \right] \tau_3. \end{aligned} \quad (5)$$

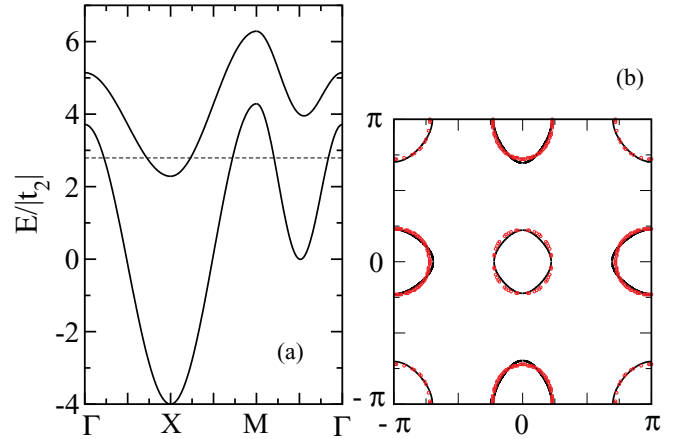


FIG. 2. (Color online) (a) Band dispersion and (b) Fermi surface of the half-filled two-orbital s model given by Eq. (5) (red circles). The continuous line is the FS for the two-orbital d model.

It is clear that here both τ_0 and τ_3 transform like A_{1g} and, for this reason, we call this model the s model. In Fig. 2, the band dispersion [Fig. 2(a)] and the FS [Fig. 2(b), red circles] are shown for the parameter values $t_1 = -0.05$, $t_2 = 0.7$, $t_3 = -0.1$, $t_4 = 0.3$, $\Delta = 2.8$, and $\mu = 1.95$. The FS of the d model is also shown (continuous black line) for comparison. They are obviously very similar, and it is precisely the goal of this effort to investigate what kinds of magnetic and pairing properties emerge from these two models that have nearly equal Fermi surfaces.

The hole pockets at the Γ and M points nest into the electron pockets at X and Y , with nesting vectors $(0, \pi)$ and $(\pi, 0)$. The system is half filled but the individual bands or orbitals are not. Note that this is the case with the orbitals in the multiorbital systems proposed for the pnictides, where nesting occurs between electron and hole pockets at the FS but none of the orbitals are exactly half filled.^{4,11}

C. Coulomb interaction

The Coulomb interaction term in both Hamiltonians is the usual one, with an on-site intraorbital (interorbital) Coulomb repulsion U (U'), a Hund coupling J satisfying the relation $U' = U - 2J$ for simplicity, and a pair-hopping term with coupling $J' = J$.³² The full interaction term is given by

$$\begin{aligned} H_{\text{int}} = & U \sum_{\mathbf{i}, a} n_{\mathbf{i}, a, \uparrow} n_{\mathbf{i}, a, \downarrow} + \frac{(U' - J/2)}{2} \sum_{\mathbf{i}, a} n_{\mathbf{i}, a} n_{\mathbf{i}, -a} \\ & - J \sum_{\mathbf{i}, a} \mathbf{S}_{\mathbf{i}, a} \cdot \mathbf{S}_{\mathbf{i}, -a} + \frac{J}{2} \sum_{\mathbf{i}, a} (d_{\mathbf{i}, a, \uparrow}^\dagger d_{\mathbf{i}, a, \downarrow}^\dagger d_{\mathbf{i}, -a, \downarrow} d_{\mathbf{i}, -a, \uparrow} \\ & + \text{H.c.}), \end{aligned} \quad (6)$$

where $d_{\mathbf{i}, a, \sigma}^\dagger$ creates an electron with spin σ at site \mathbf{i} and orbital $a = x, y$ or $1, 2$. $\mathbf{S}_{\mathbf{i}, a}$ ($n_{\mathbf{i}, a}$) is the spin (electronic density) of the orbital a at site \mathbf{i} .

To study computationally the interacting Hubbard Hamiltonian, three different many-body approaches will be used here: (i) the Lanczos technique, (ii) the real-space Hartree-Fock mean-field approximation, and (iii) the RPA. Although these methods are well known, for completeness a brief description

of these techniques is presented: (i) In the Lanczos formalism³³ the interacting Hamiltonian is exactly diagonalized in a small lattice. Taking advantage of the symmetries of the Hamiltonian, such as translational invariance, spin inversion, rotations, etc., it is possible to write the Hamiltonian matrix in a block form which allows us to obtain the lowest-energy state in each of the different Hilbert subspaces characterized by a given momentum \mathbf{k} , number of electrons, total spin projection S_z , and irreducible representations of the D_{4h} group. A comparison of the energies of all these subspaces reveals the quantum numbers of the ground state. In addition to the eigenvalues of the Hamiltonian, the Lanczos algorithm also provides the eigenvectors and, thus, the ground-state wave function can be used to calculate several different observables. The largest cluster size that can be diagonalized for the two-orbital Hubbard model has eight sites since the Hilbert subspaces, even using many symmetries, already have a large number of states between 2 and 20 million for such a cluster. These calculations are state of the art and have been carried out using a Penguin 128 GB Altus 3600 computer. Thousands of diagonalizations of the Hamiltonian were needed in order to study the two models of focus in this publication, for several values of the interaction parameters, exploring all the many Hamiltonian blocks. (ii) Another technique employed here is the real-space Hartree-Fock (HF) approximation that was briefly described in Ref. 34. The four-fermion terms in the on-site interaction portion of the Hamiltonian are decoupled using local mean-field values that are calculated self-consistently. A Hamiltonian matrix for the mean-field Hamiltonian can be constructed and this matrix is exactly diagonalized. Clusters with $N = 64$ sites can be easily studied with this technique, which is still computationally demanding since the iterative procedure used to solve the HF equations scales as $(2N)^4$. The HF Hamiltonian is too cumbersome to be reproduced in all detail here, but to guide the readers into the analytical form of its many terms the portion corresponding to the on-site intraorbital Hubbard U repulsion is reproduced:

$$\begin{aligned}
 H_U = U \sum_{\mathbf{i},a} & (\langle n_{\mathbf{i},a,\uparrow} \rangle n_{\mathbf{i},a,\downarrow} + \langle n_{\mathbf{i},a,\downarrow} \rangle n_{\mathbf{i},a,\uparrow} - \langle n_{\mathbf{i},a,\downarrow} \rangle \langle n_{\mathbf{i},a,\uparrow} \rangle \\
 & - \langle d_{\mathbf{i},a,\uparrow}^\dagger d_{\mathbf{i},a,\downarrow} \rangle d_{\mathbf{i},a,\downarrow}^\dagger d_{\mathbf{i},a,\uparrow} - \langle d_{\mathbf{i},a,\downarrow}^\dagger d_{\mathbf{i},a,\uparrow} \rangle d_{\mathbf{i},a,\uparrow}^\dagger d_{\mathbf{i},a,\downarrow} \\
 & + \langle d_{\mathbf{i},a,\uparrow}^\dagger d_{\mathbf{i},a,\downarrow} \rangle \langle d_{\mathbf{i},a,\downarrow}^\dagger d_{\mathbf{i},a,\uparrow} \rangle). \quad (7)
 \end{aligned}$$

The rest of the terms in the on-site Hubbard interaction have similar, but more complicated, expressions and they are not reproduced here. (iii) Finally, the standard RPA technique has also been employed. This diagrammatic method¹¹ is often applied to study Hubbard-like models and there is no need to reproduce the details of the approximation here. Since the interaction terms are treated perturbatively, this approach is expected to work better in the weak-coupling regime.

III. MAGNETIC PROPERTIES

For a single-orbital model, the magnetic structure factor is easily defined as

$$S(\mathbf{k}) = \sum_{\mathbf{r}} e^{i\mathbf{k}\cdot\mathbf{r}} \omega(\mathbf{r}), \quad (8)$$

with

$$\omega(\mathbf{r}) = \frac{1}{N} \sum_{\mathbf{i}} m(\mathbf{i}) m(\mathbf{i} + \mathbf{r}), \quad (9)$$

where N is the number of sites of the lattice and

$$m(\mathbf{i}) = n_{\mathbf{i},\uparrow} - n_{\mathbf{i},\downarrow} = d_{\mathbf{i},\uparrow}^\dagger d_{\mathbf{i},\uparrow} - d_{\mathbf{i},\downarrow}^\dagger d_{\mathbf{i},\downarrow}, \quad (10)$$

where $m(\mathbf{i})$ denotes the net magnetization at site \mathbf{i} .

In a multiorbital system the net magnetization at site \mathbf{i} is obtained in terms of the magnetization of each orbital a , and it is given by

$$m(\mathbf{i}) = \sum_a n_{\mathbf{i},a,\uparrow} - n_{\mathbf{i},a,\downarrow} = \sum_a (d_{\mathbf{i},a,\uparrow}^\dagger d_{\mathbf{i},a,\uparrow} - d_{\mathbf{i},a,\downarrow}^\dagger d_{\mathbf{i},a,\downarrow}). \quad (11)$$

While Eq. (11) characterizes the magnetization that is measured in experiments such as neutron scattering, it is natural to define generalized magnetic moments $m_{ab}(\mathbf{i})$ ³⁰ given by

$$m_{ab}(\mathbf{i}) = d_{\mathbf{i},a,\uparrow}^\dagger d_{\mathbf{i},b,\uparrow} - d_{\mathbf{i},a,\downarrow}^\dagger d_{\mathbf{i},b,\downarrow}. \quad (12)$$

With this definition, a generalized form of the magnetic correlation function will depend on four orbital indices:

$$\omega_{abcd}(\mathbf{r}) = \frac{1}{N} \sum_{\mathbf{i}} m_{ab}(\mathbf{i}) m_{cd}(\mathbf{i} + \mathbf{r}). \quad (13)$$

Thus, it is possible to define orbital-dependent magnetic structure factors given by

$$S_{abcd}(\mathbf{k}) = \sum_{\mathbf{r}} e^{i\mathbf{k}\cdot\mathbf{r}} \omega_{abcd}(\mathbf{r}). \quad (14)$$

These orbital-dependent operators may arise from processes as those depicted in Fig. 3(a), where having different orbitals at the two vertices is possible if the orbitals strongly hybridize to form a band.¹³

The total orbital magnetic structure factor can then be defined as

$$S_{\text{TO}}(\mathbf{k}) = \sum_{a,b,c,d} S_{abcd}(\mathbf{k}). \quad (15)$$

Note that there are M^4 orbital-dependent components of the generalized magnetic structure factor, where M is the number of active orbitals in the system. The magnetization that is measured in neutron-scattering experiments is given by

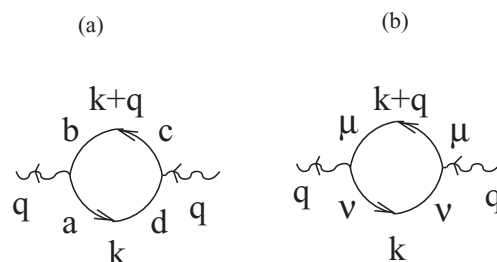


FIG. 3. (a) Electronic process that gives rise to the orbital components of the structure factor. (b) Same as shown in (a) but in the band representation.

Eq. (11), which, in terms of the components of the tensor m_{ab} , becomes

$$m(\mathbf{i}) = \sum_a n_{i,a,\uparrow} - n_{i,a,\downarrow} = \sum_a m_{aa}(\mathbf{i}) = \text{tr}[m_{ab}(\mathbf{i})]. \quad (16)$$

Since $m(\mathbf{i})$ is a trace its value is independent of the basis chosen to define the orbitals and it allows us to calculate the experimentally measured local magnetization.

Note that $m(\mathbf{i})$ is the operator that has to be considered in order to construct the so-called homogeneous or diagonal structure factor defined in terms of the diagonal (intraorbital) magnetic moments $m_{aa}(\mathbf{i})$ and given by^{11,12}

$$S_{\text{MO}}(\mathbf{k}) = \frac{1}{N} \sum_{a,b,r,i} e^{i\mathbf{k}\cdot\mathbf{r}} m_{aa}(\mathbf{i}) m_{bb}(\mathbf{i} + \mathbf{r}) = \sum_{a,b} S_{aabb}(\mathbf{k}). \quad (17)$$

S_{MO} is the physical magnetic structure factor that has to be calculated in the context of multiorbital systems to compare with neutron-scattering results.^{10,12} Several authors have pointed out the existence of the generalized components of the magnetic susceptibility both in the orbital representation^{11,35} and in the band representation.⁸ It has also been pointed out that an orbital-transverse density-wave- (OTDW) ordered state characterized by the nonhomogeneous components of the magnetization tensor may develop in multiorbital systems,³⁶ an issue that will be further explored and discussed in the present work.

A. Noninteracting case

To understand the relationship among S_{TO} , S_{MO} , and the properties of the FS of the system, it is illuminating to consider the noninteracting case that can be easily studied in momentum space. Via a Fourier transform of $d_{i,a,\sigma}^\dagger$ and $d_{i,a,\sigma}$, S_{abcd} in Eq. (14) can be written as

$$S_{abcd}(\mathbf{k}) = \sum_{\mathbf{p},\mathbf{q},\sigma,\sigma'} (-1)^{\sigma+\sigma'} d_{\mathbf{q},a,\sigma}^\dagger d_{\mathbf{q}+\mathbf{k},b,\sigma} d_{\mathbf{p},c,\sigma'}^\dagger d_{\mathbf{p}-\mathbf{k},d,\sigma'}. \quad (18)$$

In momentum space it is natural to use the band representation in which

$$\begin{aligned} S_{abcd}(\mathbf{k}) = & \sum_{\mathbf{p},\mathbf{q},\sigma,\sigma',\mu,\mu',\nu,\nu'} (-1)^{\sigma+\sigma'} \\ & \times \langle \mu|a \rangle_{\mathbf{q}} \langle b|\mu' \rangle_{\mathbf{q}+\mathbf{k}} \langle \nu|c \rangle_{\mathbf{p}} \langle d|\nu' \rangle_{\mathbf{p}-\mathbf{k}} \\ & \times d_{\mathbf{q},\mu,\sigma}^\dagger d_{\mathbf{q}+\mathbf{k},\mu',\sigma} d_{\mathbf{p},\nu,\sigma'}^\dagger d_{\mathbf{p}-\mathbf{k},\nu',\sigma'}, \end{aligned} \quad (19)$$

where $d_{\mathbf{p},\nu,\sigma}^\dagger$ creates an electron with momentum \mathbf{p} and z -spin component σ at band ν , while $\langle \nu|a \rangle_{\mathbf{p}}$ is the matrix element for the transformation from orbital to band representation.

In the band representation, the electronic processes that contribute to the magnetic correlations are shown in Fig. 3(b). Since the electronic band cannot change as the electron created at the right vertex is destroyed at the left vertex, in the band representation we can define band-dependent components of the structure factor given by

$$S_{\mu\nu\nu\mu}(\mathbf{k}) = \sum_{\mathbf{p},\mathbf{q},\sigma} d_{\mathbf{q},\mu,\sigma}^\dagger d_{\mathbf{q}+\mathbf{k},\nu,\sigma} d_{\mathbf{p},\nu,\sigma}^\dagger d_{\mathbf{p}-\mathbf{k},\mu,\sigma}, \quad (20)$$

where the Greek indices label the bands. A total structure factor can be defined in terms of $S_{\mu\nu\nu\mu}$ as

$$S_{\text{TB}}(\mathbf{k}) = \sum_{\mu,\nu} S_{\mu\nu\nu\mu}(\mathbf{k}). \quad (21)$$

Moreover, the homogeneous or diagonal magnetic structure factor S_{MB} , analogous of S_{MO} , can be defined as

$$S_{\text{MB}}(\mathbf{k}) = \sum_{\mu} S_{\mu\mu\mu\mu}(\mathbf{k}), \quad (22)$$

since in the band representation $S_{\mu\mu\nu\nu} = 0$, if $\mu \neq \nu$. Note that the band representation is the natural starting point in approaches based on fermiology.^{3,6}

In the noninteracting case being considered in this section, it is easy to show that

$$S_{\mu\nu\nu\mu}(\mathbf{k}) = 2 \sum_{\mathbf{q}} f_{\mu}(\mathbf{q}) [1 - f_{\nu}(\mathbf{q} + \mathbf{k})], \quad (23)$$

where $f_{\mu}(\mathbf{q})$ is the Fermi function for the band μ . We also find that the components of the structure factor in the orbital representation are given by

$$\begin{aligned} S_{abcd}(\mathbf{k}) = & 2 \sum_{\mathbf{q},\mu,\nu} \langle \mu|a \rangle_{\mathbf{q}} \langle b|v \rangle_{\mathbf{q}+\mathbf{k}} \\ & \times \langle v|c \rangle_{\mathbf{q}+\mathbf{k}} \langle d|\mu \rangle_{\mathbf{q}} f_{\mu}(\mathbf{q}) [1 - f_{\nu}(\mathbf{q} + \mathbf{k})]. \end{aligned} \quad (24)$$

From the expressions in Eqs. (23) and (24) it can be shown that $S_{\text{TO}} = S_{\text{TB}}$ and $S_{\text{MO}} = S_{\text{MB}}$ only if the orbitals do not hybridize to form the bands, i.e., the matrix elements are the elements of the identity matrix. In the case of a nonzero hybridization, the structure factors in the band and orbital representations then differ.

B. d model

Numerical Lanczos calculations for the homogeneous (or diagonal) magnetic structure factor S_{MO} have already been discussed in the literature for the two-orbital d model, and they indicate a tendency toward a magnetic stripe ordering for the undoped case, characterized by peaks at $\mathbf{k} = (\pi, 0)$ and $(0, \pi)$ in S_{MO} .¹² This tendency is already apparent even in the noninteracting case,^{10,12} as illustrated in Fig. 4(a), where S_{MO} calculated in a 16×16 cluster is shown with open circles, along the directions $(0, 0) - (\pi, 0) - (\pi, \pi) - (0, 0)$ in the unfolded BZ. The broad peak at $\mathbf{k} = (\pi, 0)$ is clear and it can be compared with the curve denoted by the star symbols in Fig. 4(b), where results for the $\sqrt{8} \times \sqrt{8}$ cluster that can be studied numerically exactly (with the Lanczos algorithm and for any value of the Hubbard couplings) are presented. This same behavior is also apparent in the total orbital structure factor $S_{\text{TO}}(\mathbf{k})$ indicated by the diamonds in Fig. 4(a).

On the other hand, a calculation of the magnetic structure factor using the band representation, i.e., $S_{\text{MB}}(\mathbf{k})$, indicated by the squares in Fig. 4(a), shows a rather different behavior: Instead of a clear peak at $(\pi, 0)$, there is a featureless plateau around $(\pi, 0)$ that extends to $(\pi/2, \pi/2)$. This example demonstrates the importance of the matrix elements in Eq. (19) that differentiate between S_{MO} and S_{MB} . In the noninteracting case, both functions can be expressed in terms of the Fermi functions as in Eqs. (23) and (24), allowing us to conclude that

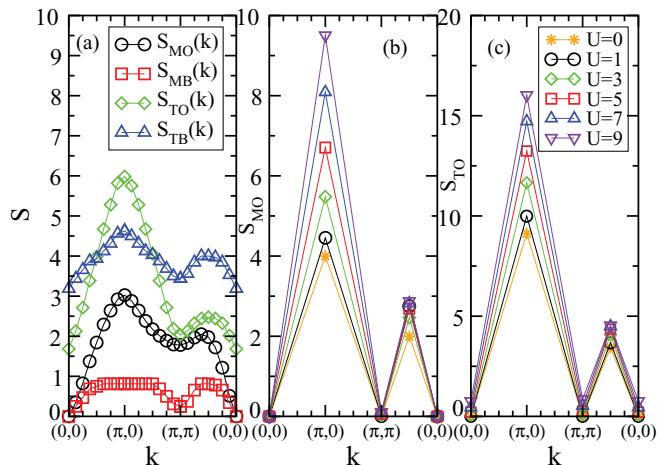


FIG. 4. (Color online) (a) Magnetic structure factors, total and homogeneous as indicated, for the noninteracting two-orbital d model on a 16×16 lattice. (b) Homogeneous orbital magnetic structure factor $S_{MO}(\mathbf{k})$ for the interacting case with $J/U = 0.25$ and at the indicated values of U . The results were obtained numerically using an eight-site cluster and the Lanczos method. (c) Total orbital magnetic structure factor $S_{TO}(\mathbf{k})$ for the interacting case for the same parameters and technique used in (b).

the peak at $(\pi, 0)$ arises from the matrix elements rather than from purely nesting effects of the Fermi surfaces. Ignoring the matrix elements, it is interesting to note that a feature at $(\pi, 0)$ can also develop if all the components of the structure factor in the band representation are considered and $S_{TB}(\mathbf{k})$ is calculated, as shown by the curve indicated with triangles in Fig. 4(a).

The contribution of the band- and orbital-resolved components of the structure factor in the noninteracting case are presented in Fig. 5(a). The components of the structure factor that contribute to S_{MO} are S_{aabb} with a (b) taking the values x (y) and y (x) indicated by the diamonds in the figure, and S_{aaaa} (indicated by the circles and squares). It is clear from the figure that the peak at $(\pi, 0)$ in S_{MO} at the noninteracting level is mostly due to the S_{aabb} that arise from the nesting of the two bands that contain the same orbital flavors due to hybridization, while the components of the form S_{aaaa} show features also at (π, π) since this wave vector also nests the hole (electron) FS's at Γ and M (X and Y). It can be seen that the nonhomogeneous components of the form S_{abab} (diamonds) behave as S_{aabb} in the noninteracting case and contribute to form the peak at $(\pi, 0)$ in the total structure factor S_{TO} [triangles in Fig. 4(a)]. For completeness, in Fig. 5(a) orbital-resolved structure factors of the form S_{abba} (up-triangles) and S_{abbb} (down-triangles) are also shown; S_{abba} increases the value of S_{TO} at $(\pi, 0)$ while S_{abbb} provides a small negative contribution to S_{TO} along the diagonal direction of the BZ. Similar results were obtained for all the correlations in which three of the four indices are the same.

In noninteracting single-orbital systems, as studied for the cuprates, the spin and charge susceptibilities have the same form for all values of nonzero momenta, and any features in these functions arise from the nesting properties of the Fermi surface. Naively, the same is expected in the case of multiorbital models but, as discussed below, the hybridization

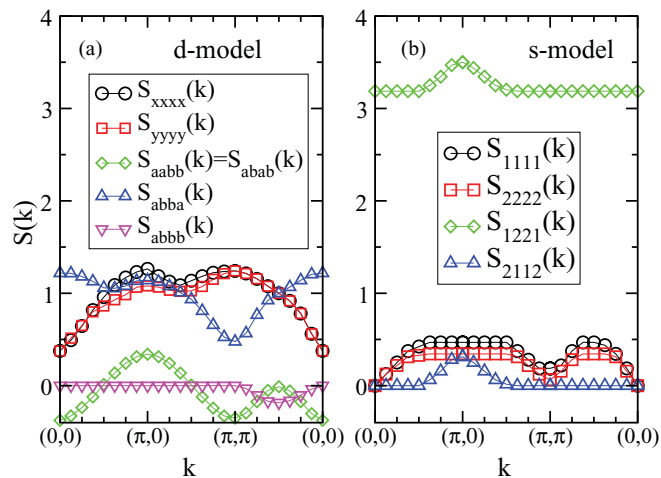


FIG. 5. (Color online) (a) Orbital-resolved components of the magnetic structure factor for the noninteracting two-orbital d model on a 16×16 lattice. (b) Band- (orbital-) resolved components of the magnetic structure factor for the noninteracting two-orbital s model also on a 16×16 lattice. The index 1 (2) labels the lower (upper) band.

of the orbitals plays a crucial role. In the d model, the peaks in S_{MO} appear to be associated with the nesting of the hole- and electron-like Fermi surfaces. In the weak-coupling picture, it is expected that magnetic order with \mathbf{Q} equal to the nesting moments stabilizes when repulsive Coulomb interactions are added. Our Lanczos calculations for S_{MO} and S_{TO} , in Figs. 4(b) and 4(c), show that this is indeed the case.

The Lanczos calculated orbital magnetic structure factor $S_{MO}(\mathbf{k})$, using a $\sqrt{8} \times \sqrt{8}$ sites cluster, is shown in Fig. 4(b) for different values of U and at $J/U = 0.25$. This structure factor has a peak at $\mathbf{k} = (\pi, 0)$ [and $(0, \pi)$ as well, not shown] that becomes sharper as U increases, indicating a tendency toward robust magnetic order. Mean-field calculations based on these results, but extended to much larger systems, indicate that actual magnetic order develops at a finite value of U .^{12,14} The Lanczos-evaluated behavior of the $S_{MO}(\mathbf{k})$ peak at $\mathbf{k} = (\pi, 0)$, as a function of U , is shown in Fig. 6(a) for two different values of J/U (0.05 and 0.25). The tendency toward a robust magnetic state with increasing U and J/U is again clear.

As previously stated, S_{MO} is the magnetic structure factor calculated in the literature for comparison with experiments, but for completeness and for the sake of comparison with the s -model results, in Fig. 4(c) we present the Lanczos calculated values for the total generalized magnetic moment S_{TO} for the d model as a function of U , for the case $J/U = 0.25$. It is clear that for the d -model S_{TO} mimics the behavior of S_{MO} . An important question to ask is what are the components of the orbital-resolved magnetic structure factor that drive the development of a peak at $\mathbf{Q} = (\pi, 0)$ [and $(0, \pi)$] when the Coulomb interactions are active. In Fig. 7 partial sums over selected components of the structure factor are shown with summations performed over repeated indices. In Fig. 7(a) it can be clearly observed that S_{aabb} , whose sum over a and b are indicated by the plus signs and the continuous lines in different shades for the different values of the interaction, are the

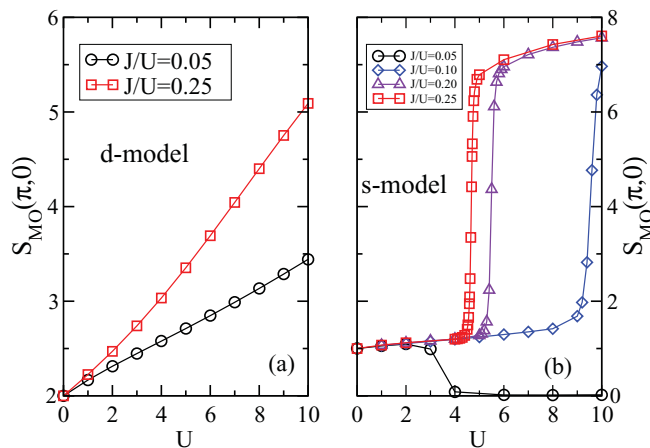


FIG. 6. (Color online) Orbital magnetic structure factor at wave vector $(\pi, 0)$ calculated numerically (Lanczos). (a) Results for the two-orbital d model as a function of the Coulomb repulsion U and for the values of J/U indicated. (b) Same as (a) but for the s model.

components that drive that magnetic behavior. In fact, these are the homogeneous components that contribute to the physical magnetic structure factor S_{MO} . It is interesting to note that while $\sum_{a,b} S_{aabb}$ is equal to $\sum_{a,b} S_{abab}$ in the noninteracting system [Fig. 5(a)] the partial sum of the nonhomogeneous component $\sum_{a,b} S_{abab}$ [x symbols and dotted lines in Fig. 7(a)] does not increase with U at \mathbf{Q} while the partial sum $\sum_{a,b} S_{aabb}$ clearly does.

C. s model

Let us now carry out a similar analysis but for the two-orbital s model defined by Eq. (5). Since in this model each band is defined by a single orbital, it is then clear that $S_{MO} = S_{MB}$ and $S_{TO} = S_{TB}$.³⁷ Note that studies based on

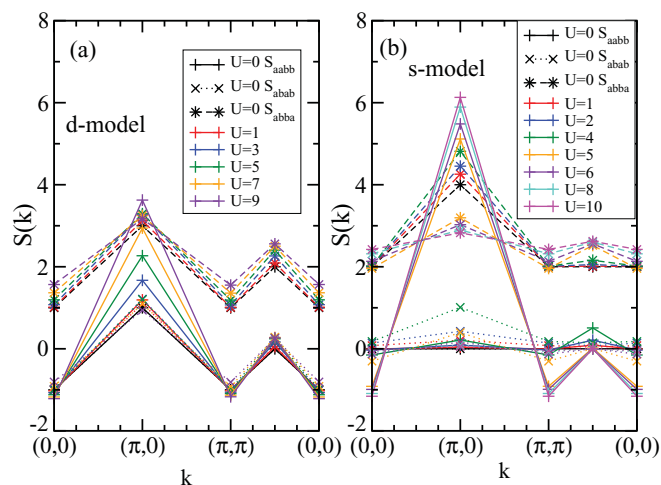


FIG. 7. (Color online) Orbital-resolved components of the total structure factor (sums over repeated indices are implied): S_{aabb} (plus sign, solid line), S_{abab} (x, dotted line), and S_{abba} (asterisk, dashed line) for the values of U indicated, obtained numerically (Lanczos) at $J/U = 0.25$ using an eight-site cluster for (a) the d model and (b) the s model.

fermiology assume that if hole and electron FS's are nested via a momentum vector \mathbf{Q} , then spin-density wave order will arise from a logarithmic instability that develops in the spin response at \mathbf{Q} and is stabilized by the Coulomb interaction.^{3,6} In this scenario the spin-density wave originates from the formation of particle-hole pairs, excitons, belonging to the electron and hole FS's (excitonic mechanism).⁶ Our goal is to investigate whether this mechanism is valid for the s model.

The magnetic structure factor S_{MO} in the noninteracting limit, denoted by the squares in Fig. 8(a), does not show the features expected from the nesting of the two Fermi surfaces at momentum \mathbf{Q} . The structure factor is actually rather flat on all the BZ, vanishing at $\mathbf{k} = (0, 0)$ and (π, π) . These results are not what would have been expected from the nesting properties.

Note that the results for S_{MO} in the noninteracting s model [squares in Fig. 8(a)] are actually identical to the results for the homogeneous structure factor in the d model in the band representation S_{MB} [indicated by squares in Fig. 4(a)], since both systems have the same FS. However, note how the results for the d model in the orbital representation differ [indicated by circles in Fig. 4(a)]. This is due to the effect of the matrix elements that result from the hybridization of the orbitals, which play a crucial role in the magnetic properties of the system. This effect can be more clearly appreciated when the interactions are added. The behavior of the peak in $S_{MO}(\mathbf{k})$ at $\mathbf{k} = (\pi, 0)$ was calculated with the Lanczos method applied to the s model by varying U and at different values of J/U using an $N = 8$ sites tilted cluster. In Fig. 6(b) it can be observed that for values of $J < 0.1U$ the peak in S_{MO} eventually vanishes. On the other hand, for $J \geq 0.1U$, a rapid increase in the peak's magnitude suddenly occurs at a value of U that decreases as J/U increases. The increase of the peak at $(\pi, 0)$ with increasing U is contrasted with the behavior of the feature at $(\pi/2, \pi/2)$ displayed in

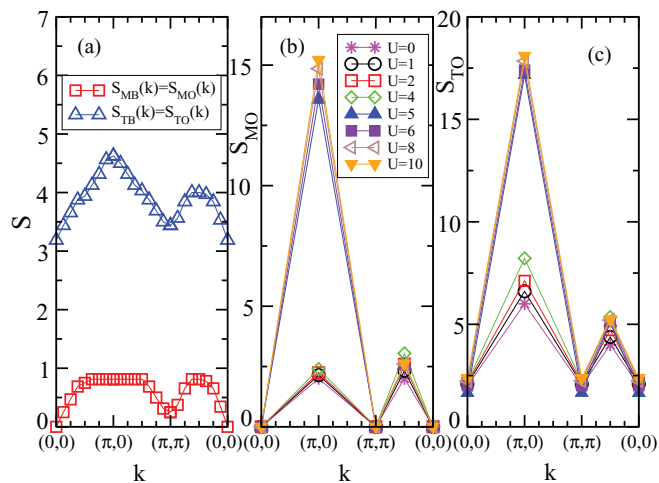


FIG. 8. (Color online) (a) Magnetic structure factors (total and homogeneous) as indicated for the noninteracting two-orbital s model using a 16×16 lattice. (b) Homogeneous orbital or band magnetic structure factor $S_{MO}(\mathbf{k})$ for the interacting case with $J/U = 0.25$ at the indicated values of U . The results were obtained numerically via the Lanczos method using an eight-site cluster. (c) Total orbital or band magnetic structure factor $S_{TO}(\mathbf{k})$ for the interacting case with the same parameters as in (b).

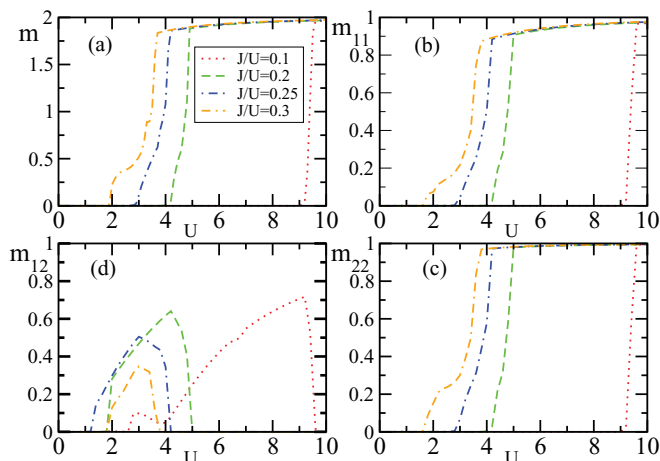


FIG. 9. (Color online) Mean-field calculated orbital- or band-resolved magnetic order parameters for the s model, as a function of U and for the indicated values of J/U . (a) Total homogeneous magnetic order parameter $m = m_{11} + m_{22}$; (b) m_{11} ; (c) m_{22} ; (d) $m_{12} = m_{21}$.

Fig. 8(b). Examination of the numerical (Lanczos) ground state indicates that, at this point, the Hubbard interaction is strong enough to hybridize the two bands and develop magnetic stripe order.

Based on the numerical results discussed above, a Hartree-Fock mean-field calculation was performed, following technical aspects already discussed briefly in previous literature.^{14,34} By this procedure we found that the total (homogeneous) magnetization m shown in Fig. 9(a) mimics the behavior of $S_{\text{MO}}(\pi, 0)$. The transition to the magnetically ordered state is very rapid, resembling a first-order transition. We observed that MF magnetic order develops only if $J \geq 0.1U$, which is in agreement with the Lanczos results shown in Fig. 6(b). The mean-field results also indicate that a full gap characterizes the magnetic state that is then an insulator as it can be seen from the MF calculated spectral functions $A(\mathbf{k}, \omega)$ displayed in Fig. 10(a). It is clear that the hybridization of the original bands or orbitals due to the Coulomb interaction is very strong and the band structure has been totally reconstructed. This behavior can be understood in the real-space representation. In order to develop magnetic stripes in the half-filled system, it is necessary to have a net magnetic moment on each site. In the d model, each orbital is half filled and thus contains a spin-1/2 that can easily be polarized by the interaction. In the s model, on the other hand, the orbitals correspond to the bands, and one orbital is thus almost filled while the other is almost empty. Then, there are far fewer magnetic moments that can be polarized.

Thus, we observe that in the s model the peak at \mathbf{Q} in the magnetic structure factor does not develop from the nesting of the FS but from the Coulomb interaction, and it occurs fairly suddenly and at a robust value of $U \geq 4$ for the hopping parameters used here. Thus, while nesting appears to be a needed condition for the development of the peak in the magnetic structure factor, it is not a sufficient condition. The hybridization of the orbitals needs to be present such that the matrix elements allow the peak to emerge at sufficiently strong coupling. In fact, it is necessary that the bands that

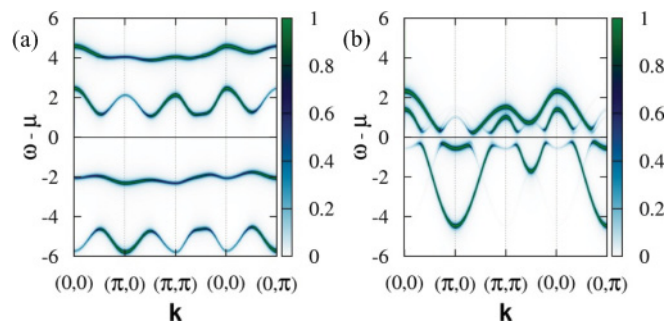


FIG. 10. (Color online) Intensity of the mean-field calculated spectral functions $A(\mathbf{k}, \omega)$ as a function of $\omega - \mu$ and \mathbf{k} for the s model: (a) in the stripe magnetic phase for $U = 5$ and $J/U = 0.25$; (b) in the phase with orbital-transverse spin order for $U = 2.5$ and $J/U = 0.25$.

are connected by the nesting vector \mathbf{Q} share the same orbital flavor. If this occurs via hybridization, magnetic order can develop at relatively weak coupling, but if this is not the case, the Coulomb interaction would induce magnetic order only in the strong-coupling regime, as we have verified by studying the s model. In this case, the magnetic transition is also a metal-insulator transition, as observed at least within the mean-field approximation. The d -orbital model, on the other hand, is known to display an intermediate metallic magnetic phase.¹⁴ Thus, the present results indicate that the s and d models develop similar magnetic behavior only in the strong-coupling regime while in weak coupling, despite the nearly identical Fermi surfaces, both models have quite different ground states.

1. Orbital-transverse spin order

While the analysis of the results for the s model presented above indicates that, despite the nesting of the electron and hole FS's, no magnetic order, as defined by the homogeneous operator, develops in weak coupling, it is instructive to analyze the behavior of the nonhomogeneous components and the total magnetic structure factor S_{TO} . The noninteracting values of S_{TO} on a 16×16 lattice are indicated by the triangles in Fig. 8(a). There is a feature at $(\pi, 0)$ arising from the contribution of the interband components of the form $S_{abba} \equiv S_{\mu\nu\nu\mu}$, shown by the triangles and diamonds in Fig. 5(b). These are the components of S_{abcd} that contribute to the development of the maximum at $\mathbf{Q} = (\pi, 0)$ [and $(0, \pi)$] because the nesting at \mathbf{Q} is between FS's defined by different bands. However, these type of terms are not part of the definition of the homogeneous structure factor S_{MB} . On the other hand, the components of the form S_{aaaa} , indicated with circles and squares in Fig. 5(b), have a very flat shape in all the BZ and do not produce a sharp feature. Any other combination of orbital indices does not contribute to S_{TO} as shown in Eq. (23).

The effect of the Coulomb interactions on the feature at $(\pi, 0)$ in S_{TO} has been obtained with Lanczos calculations and it can be seen in Fig. 8(c). The peak slowly increases as U increases from 0 to 4. Note that for the same range of values of U the peak in S_{MO} shown in Fig. 8(b) does not change. The obvious question is whether this behavior indicates a novel kind of order in multiorbital systems.

The answer is provided via our MF approach that allows us to evaluate the components of the magnetization m_{ab} . The homogeneous magnetization m displayed in Fig. 9(a) is obtained as the sum of the intraorbital magnetizations m_{11} and m_{22} shown in Figs. 9(b) and 9(c). Interestingly, we found that the nondiagonal components $m_{12} = m_{21}$ develop finite values while the diagonal components are zero for values of $J/U > 0.1$ as shown in Fig. 9(d). At the MF level we can study the real space configuration associated to this finite-order parameter. We have observed that the orbital spins are disordered, which is expected by the lack of features in $S_{\text{MO}}(\mathbf{k})$, but there are ordered generalized spins $\mathbf{G}_{ab}(\mathbf{i})$ defined as

$$\mathbf{G}_{ab}(\mathbf{i}) = d_{i,a,\alpha}^\dagger \vec{\sigma}_{\alpha,\beta} d_{i,b,\beta}, \quad (25)$$

where $\vec{\sigma}$ are the Pauli matrices and the orbital indices $a \neq b$. In Fig. 11 we show two configurations of $\mathbf{G}_{12}(\mathbf{i})$ that provide the MF ground state associated with the peak in S_{TO} at $(\pi, 0)$ [and $(0, \pi)$] when m_{12} is finite. Figure 11(a) shows a flux configuration that generates peaks at $(\pi, 0)$ and $(0, \pi)$ in S_{TO} and Fig. 11(b) shows a stripe configuration that produces a peak at $(0, \pi)$. The peak at $(\pi, 0)$ is generated by a companion configuration rotated by $\pi/2$. Flux and stripe configurations have energies very close to each other and the actual ground state depends on the parameters.³⁸

The new phase hinted at by the Lanczos calculations and stabilized in the MF calculations is insulating. The MF calculated spectral functions are shown in Fig. 10(b). A full gap has developed at the FS, indicating that this order, if realized, would be observed with ARPES measurements. On the other hand, neutron-scattering experiments would not detect it. This can be seen by performing a rotation in orbital space given by³⁶

$$d_{i,\pm,\sigma}^\dagger = \frac{1}{\sqrt{2}}(d_{i,1,\sigma}^\dagger \pm d_{i,2,\sigma}^\dagger). \quad (26)$$

In this new basis the schematic representations of the spins are shown in Fig. 12. It is clear that while the homogeneous spins in the orbitals + (black dots) and - (white dots) are ordered, the net spin at each site is 0 and, thus, neutron-scattering experiments will not detect the order because there

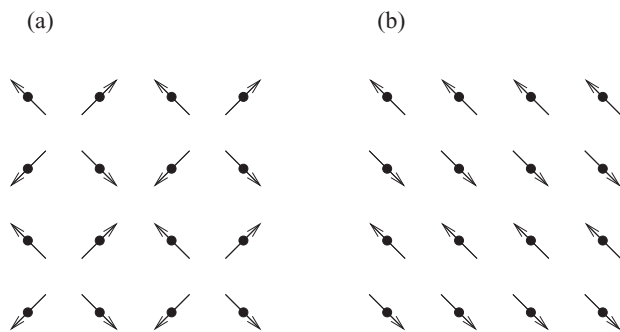


FIG. 11. Schematic representation of the real-space mean-field calculated ground states for the s model when m_{12} is nonzero. (a) Flux phase; (b) stripe phase. The dots indicate the sites and the arrows represent the MF value of the generalized spin $\mathbf{G}_{12}(\mathbf{i})$ defined in the text.

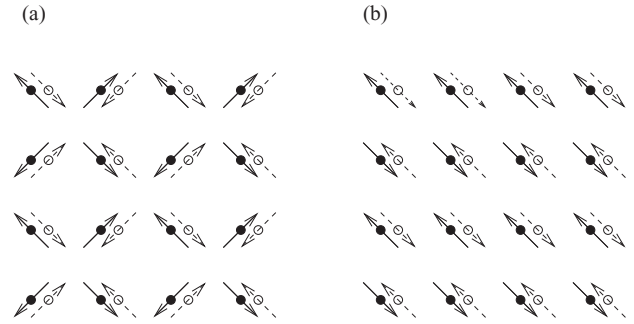


FIG. 12. Schematic representation of the real-space mean-field calculated ground states for the s model when m_{12} is nonzero: (a) flux phase; (b) magnetic stripe phase. The black and white dots represent the orbitals + and - at each site and the continuous and dashed arrows represent the MF value of the spin at each orbital.

is no finite local magnetization. These phases appear to be a realization of the orbital-transverse density-wave (OTDW) order proposed in Ref. 36.

Summarizing, a careful analysis of the small-cluster ground states obtained via Lanczos techniques, and with mean-field approximations in larger clusters, highlights the important role that the orbital composition plays in the development of magnetic order.

For the s model, it is illuminating to consider the behavior of the total magnetic structure factor S_{TO} , see Fig. 8(c), calculated numerically as the interactions are increased. There is a weak increase of S_{TO} at \mathbf{Q} before the sudden jump at $U = 4$. The behavior of the resolved components displayed in Fig. 7(b) shows that for $0 \leq U \leq 4$ the partial sum over a and b of the nonhomogeneous components S_{abab} (x symbols and dotted line) and S_{abba} (asterisk symbols and dashed lines) increases in value at $(\pi, 0)$ indicating the stabilization of the orbital-transverse spin phase. For $U > 4$ a sudden increase of the sum of the homogeneous components S_{aabb} (plus symbols and continuous line) develops, the nonhomogeneous components start to decrease, and homogeneous magnetic order is established.

D. Weak coupling: RPA analysis

Additional insight into the weak-coupling behavior of the d and s models can be obtained via the diagrammatic RPA method. Using this technique, the magnetic susceptibility $\chi_{abcd}(\mathbf{k}, i\omega)$ was calculated,^{11,13} and the static structure factor was obtained by integrating the results over ω .³⁹ In Fig. 13(a), the RPA-calculated diagonal or homogeneous structure factor for the d model is presented. The noninteracting result [in agreement with the results indicated by the circles in Fig. 4(a)] are denoted by the dashed line, while results at $U = 2.64$, the coupling strength where divergent behavior is about to occur for the case $J/U = 0.25$, are indicated by the solid line. In these results the peak at $(\pi, 0)$ is very prominent both with and without the Hubbard interaction on.

The same calculation performed for the s model, presented in Fig. 13(b), gives rather different results. The flat behavior in the noninteracting case (dashed line), in agreement with the curve indicated by squares in Fig. 8(a), is replaced within the

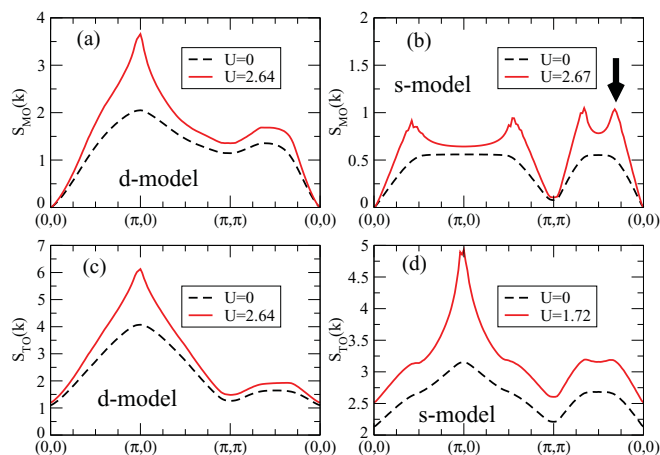


FIG. 13. (Color online) RPA calculated magnetic structure factors for $J/U = 0.25$, at the values of U indicated (full line). The noninteracting results are indicated with dashed lines. (a) Homogeneous magnetic structure factor in the d model. (b) Same as shown in (a) but for the s model. The arrow indicates the peak that grows the most as the critical U is reached. (c) Generalized magnetic structure factor for the d model. (d) Same as shown in (c) but for the s model.

RPA by a curve (continuous line) that develops weak features at incommensurate values of the momentum. Note that there were no precursors of these features in the noninteracting limit. Eventually the peak the closest to the Γ point along the diagonal direction of the BZ, indicated with an arrow in the figure, was found to diverge when U becomes larger than 2.67 for $J/U = 0.25$. This appears to be an illustration of a case in which RPA calculations indicate magnetic behavior that is unrelated to nesting properties. The RPA results show that an excitonic weak-coupling picture in which magnetic order characterized by the nesting momentum \mathbf{Q} is expected to occur can be misleading if the orbital composition of the bands is not incorporated into the discussion. In the excitonic picture, the expectation is that the Coulomb interaction will allow the formation of electron-hole pairs with the electron (hole) in the electron (hole) Fermi surface. Since S_{MO} incorporates intraorbital electron-hole pairs, an RPA response requires that the nesting vector connects parts of the electron and hole bands that contain the *same* orbital flavor. This is the case in the d model where, even in the weak-coupling regime, the $(\pi, 0)$ magnetic-stripe state with two electrons with parallel spins at every site of the lattice has the largest weight in the ground state according to our Lanczos numerical studies. Since both orbitals are degenerate, the energetic penalization for populating both orbitals is U' and there is a gain given by J if both spins are parallel. As discussed before, in the s model, on the other hand, the orbitals are nondegenerate and, thus, in addition to U' there is an energy Δ of penalization when two electrons are located in different orbitals at the same site. This energy can be larger than the gain obtained from J by having parallel spins or than the U penalization that arises from introducing both electrons in the same orbital. Then, a magnetic “stripe” state can only develop when U is comparable to the splitting Δ . This regime, which develops in strong coupling according to our Lanczos and MF calculations, is not captured by the weak-coupling RPA method. However, it will

be shown that RPA is effective at finding the orbital-transverse spin state presented in the previous section if the generalized structure factor S_{TO} is calculated.

The values of S_{TO} obtained with RPA are presented in Figs. 13(c) and 13(d) for the d and s models, respectively. Both develop a peak at the nesting wave vector. The generalized structure factor takes into account electron-hole pairs formed by an electron and a hole in different bands that are allowed to have different orbital flavors. This is the reason why a peak develops now in both cases. While in the case of the d model the behavior of S_{TO} mimics S_{MO} and the divergence in both occurs at the same value of U (slightly above 2.64 for $J/U = 0.25$), indicating that the stripe-magnetic order is the cause, in the s model, the peak in S_{TO} develops at a lower value of U ($U = 1.72$ for $J/U = 0.25$) and it results from the ordering revealed by the inhomogeneous components S_{1221} and S_{2112} of the structure factor, i.e., orbital-transverse spin order as discussed in the previous section. In this new light, we see that the divergence in S_{MO} should be disregarded since it occurs for a much larger value of U than the divergence in S_{TO} . These results show that if all the elements of the susceptibility tensor are considered, RPA calculations are able to determine the development of new ordered phases that can develop in multiorbital systems. Conversely, in multiorbital systems in which orbital-transverse order develops, RPA calculations using only the homogeneous susceptibility may lead to unphysical results.

E. Strong-coupling regime

In the regime where the coupling U is sufficiently strong such that even in the s model it is energetically favorable to locate two electrons with parallel spins at the same site (and in different orbitals), both the s and d models can be mapped into effective $t - J - J'$ models and an insulating state with magnetic stripes can occur. In this case, the Hubbard repulsion has effectively hybridized both bands causing large distortions and actually opening a full gap [see Fig. 10(a)]. In this strong-coupling regime both models appear to have similar properties, but an insulating magnetic behavior does not reproduce the experimental behavior observed in several of the undoped iron pnictides (such as the 1111 and 122 families). However, this regime could be applied to the chalcogenides: if U is sufficiently strong the magnetic behavior that develops in the strong-coupling limit is more related to the hopping parameters and superexchange than to the weak-coupling nesting properties of the Fermi surface. While the values of the hopping parameters in the Hamiltonian are crucial to achieve nesting in weak coupling,³⁵ systems in which nesting is not perfect can develop stripelike magnetic order if they map into a $t - J - J'$ model in the strong-coupling limit such as in the case of the three-orbital model for the pnictides.¹⁵

The results in this section indicate that in the case of the pnictides, even if the five d orbitals are considered, the xz and yz orbitals are the most likely to produce the strongest contribution to the metallic stripe magnetic order at weak or intermediate values of the Hubbard interaction because they are the major constituents of the FS's with better nesting and because they are degenerate and, thus, there is no energy Δ that needs to be overcome by the interaction. This is apparent

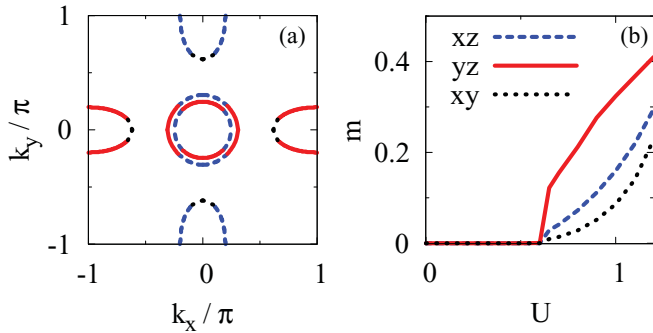


FIG. 14. (Color online) (a) Fermi surface with its orbital composition for the case of a three-orbital model for the pnictides. (b) Mean-field calculated orbital-resolved magnetization for the same three-orbital model. The figure was taken from Ref. 15 for illustration.

in the three-orbital model for the pnictides, where a mean-field calculation shows that magnetic order develops at a finite value of U [see Fig. 14(b)].¹⁵ In Fig. 14(a) it can be observed that the orbital with the best nesting associated with $\mathbf{Q} = (\pi, 0)$ is the yz one, indicated by the continuous line. A mean-field calculation of the orbital-resolved magnetization m_{aa} for $a = xz, yz$, and xy shows that $m_{yz,yz}$ grows very rapidly at the lowest value of U . The magnetizations for the other orbitals develop as U hybridizes and distorts the original bands. Thus, in the intermediate U regime when magnetism develops, the xz and yz orbitals are the ones that would develop the stronger magnetization (albeit for different values of \mathbf{Q}), giving rise to a magnetic metallic phase. Thus, nesting seems to drive the magnetization of the xz/yz orbitals while the additional orbital hybridizations that develop due to the reconstruction of the FS then drives the smaller magnetization in the remaining orbitals.

IV. PAIRING SYMMETRIES

Regarding the symmetry of the pairing operators corresponding to the models analyzed here, previous numerical calculations have indicated competition among the A_{1g} , B_{2g} , and E_g states in the d model,^{12,40} as shown in Fig. 15(a). The E_g states correspond to a p -wave spin-triplet state that becomes destabilized on the addition of binding-enhancing Heisenberg terms.⁴⁰ The favored pairing operators with the symmetry A_{1g} are all trivial in their orbital composition, i.e., they are intraorbital with the form $D^\dagger \sigma_0 D$, where $D^\dagger = (d_{\mathbf{k},x,\uparrow}^\dagger, d_{-\mathbf{k},y,\downarrow}^\dagger)$ in the (x, y) basis, and they remain intraorbital in the (X, Y) basis. However, the B_{2g} pairing operators have a nontrivial orbital composition given by $D^\dagger \sigma_1 D$ in the basis (x, y) , indicating that the pairs are made of electrons in the two different orbitals. In the (X, Y) basis the B_{2g} pairing operator becomes $D^\dagger \sigma_3 D'$ with $D'^\dagger = (d_{\mathbf{k},X,\uparrow}^\dagger, d_{-\mathbf{k},Y,\downarrow}^\dagger)$. Thus, in the (X, Y) representation the B_{2g} pairs are intraorbital but there is an important sign difference between the pairs in the different orbitals that makes the orbital contribution intraorbital but nontrivial. It is interesting to observe that the intraorbital B_{1g} state found with RPA calculations in the five-orbital model for the pnictides¹¹ would become interorbital in the (X, Y) basis.

The results for the s model regarding pairing properties differ from those in the d model. Following previous

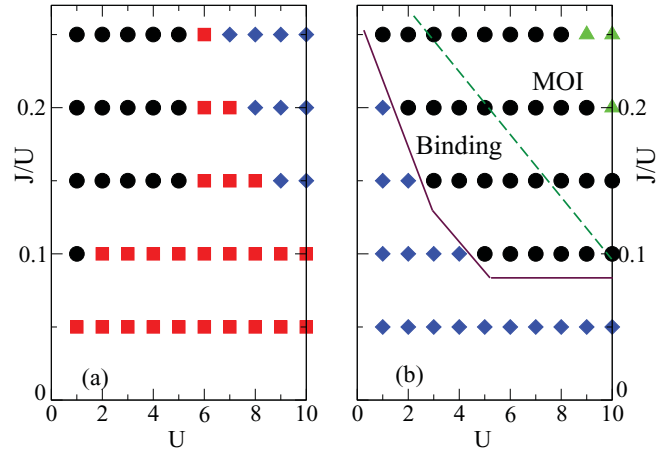


FIG. 15. (Color online) (a) Relative symmetry between the undoped and the electron-doped ground states for the case of the d -orbital model, varying J/U and U . The results were obtained numerically via the Lanczos method using a small cluster with $N = 8$ sites (and following steps already discussed in previous literature).^{10,40} The circles indicate states with E_g symmetry, squares correspond to B_{2g} , and diamonds represent A_{1g} symmetric states. (b) Same as shown in (a) but for the s model with the triangles denoting B_{1g} symmetry. In the region above the continuous line the two added electrons form a bound state. The dashed line indicates the boundary for the stability of the magnetically ordered insulating (MOI) region in the undoped state.

investigations,¹⁰ using the Lanczos method we have calculated the relative symmetry between the undoped (number of electrons $N_e = 16$) and electron-doped ($N_e = 18$) states, as an indicator of the possible pairing symmetry in the bulk limit. More specifically, the ground state in the subspace of 16 and 18 electrons was obtained with the Lanczos technique described in Sec. II C. Since the diagonalizations are carried out in subspaces of the Hilbert space expanded by states that transform according to a well-determined irreducible representation of the group D_{4h} , then it is simple to determine the relative symmetry between the ground states for 16 and 18 electrons. The results are presented in Fig. 15(b), varying U and J/U . For small values of U and J/U the doped ground state has symmetry A_{1g} in agreement with the d model, although in a different regime of couplings. Increasing U and J/U , the s -model ground state switches to the E_g symmetry, i.e., p wave. This p symmetry arises from the spatial location of the electrons since the orbital contribution is trivial. We have observed that in the small cluster studied here the spin-triplet state with $\mathbf{k} = (0, 0)$ is almost degenerate with a spin-singlet state with $\mathbf{k} = (\pi, \pi)$. The possibility of having a spin-singlet p -wave state with wave vector $\mathbf{k} = (\pi, \pi)$ has been previously discussed long ago in the context of the single-orbital Hubbard model.⁴¹ In the present case, we need to remember that \mathbf{k} is a pseudomomentum and in the folded representation $\mathbf{k} = (\pi, \pi)$ actually maps into $(0, 0)$ so the actual Cooper pair, if stabilized, has zero center-of-mass momentum, but the components of the pair belong to bonding and antibonding bands that could become hybridized for the large values of the interactions needed to stabilize these states. As indicated in the figure, it was also found that the p states show binding in the small

system studied here. In addition, a small region of bound states with B_{1g} symmetry is found at even larger couplings. While in the d model our numerical results indicate that the orbital degree of freedom plays a crucial role in the symmetry of the pairing states, we observe that this is not the case in the s model. This result seems to indicate that interorbital Cooper pairs are likely to be present in multiorbital systems with strongly hybridized bands as is the case for the pnictides.

Understanding more deeply why the s model develops its particular pairing properties is at this point unnecessary since the model simply provides an illustration of a system with a similar FS as the d model, and the goal of this work was to show that the orbital composition of the bands plays a crucial role in determining the symmetry of the doped states. The examples that have been discussed here clearly show that models with the same Fermi surface and the same interactions can have very different pairing properties depending on the degree of hybridization of the orbitals. It also seems, according to the present results, that the relevance of the orbital degree of freedom in determining the pairing symmetry is also influenced by the degree of hybridization among those orbitals.

V. CONCLUSIONS

To summarize, numerical and analytical calculations were performed in order to compare the properties of two-band models with identical FS's and interactions but differing in the degree of hybridization of the orbitals to form the bands. Despite the nesting properties of the FS's it was discovered that both models have similar magnetic (insulating) ground states in the strong-coupling limit, but they differ in weak and intermediate coupling. The s model offers an example in which, despite the nesting of the FS and the presence of Coulomb interactions, magnetism does not develop in weak coupling. However, it was discovered that, instead, as a result of the nesting in weak coupling, the Coulomb interaction stabilizes an orbital-transverse spin-ordered state with no local magnetization. This state is insulating and is characterized by a gap that could be observed in ARPES experiments. However, due to the lack of local magnetization, neutron-scattering experiments would not detect the development of "generalized spin order." In fact, standard RPA calculations in the s model lead to incorrect results such as incommensurate magnetic order in the physical homogeneous channel. However, when the nonhomogeneous components of the susceptibility are taken into account, RPA reveals the existence of the orbital-transverse spin phase for values of U lower than the ones needed to observe the unphysical magnetic state. It is clear that the physical (homogeneous) magnetic structure factor depends strongly on the orbital flavor of the bands and for this quantity to develop a peak in weak coupling it is necessary that the

portions of the FS connected by nesting have the same orbital flavor.

The possibility of "hidden" magnetic ordering in the pnictides has been proposed by several authors⁴²⁻⁴⁴ as an explanation for the unexpectedly low value of the magnetization in several of these materials. The hidden order proposed by these authors was "diagonal," as the configurations we presented in Fig. 12 after transforming our nondiagonal results into a rotated orbital basis. However, in multiorbital systems with more than two orbitals, it may be necessary to consider the nondiagonal order as well. In theoretical and analytical calculations these nondiagonal hidden orders are revealed by considering all the components, homogeneous and inhomogeneous, of the magnetic susceptibility. On the experimental side, ARPES can detect gaps that are opened due to the "hidden" magnetic order but the traditionally used techniques to detect homogeneous magnetic order, such as neutron scattering, will fail due to the lack of a local magnetization.

We also found indications of quenching of the orbital degree of freedom in systems with nonhybridized orbitals. The orbitals do not appear to play a role in determining the symmetry of the pairing states. This degree of freedom, though, is crucial in systems with hybridized orbitals. In the case of the pnictides in particular, we have shown that the ground states with d symmetry found in the literature in models for the pnictides, such as the B_{1g} , can be made interorbital by changing the basis in which the degenerate xz and yz orbitals are defined.

The results provided by this work may explain why the end member of the series $\text{BaFe}_2(\text{As}_{1-x}\text{P}_x)_2$ is nonsuperconducting despite displaying the best nesting of all the compounds in the series.²⁹ If superconductivity necessitates magnetic fluctuations they may not be sufficiently strong in this compound if there is no good matching between the flavor of the orbitals in the nested bands.

Finally, our results confirm the perception expressed in the analysis of recent photoemission experiments²⁸ that the weak-coupling nesting mechanism would not be applicable if, indeed, a hole-pocket band dominated by the orbital $3z^2 - r^2$ (with no nesting partner in the electron-pocket band) develops a robust superconducting gap. Confirming and then understanding the results of those recent photoemission experiments is very important for the clarification of several intriguing issues in the challenging physics of the pnictides.

ACKNOWLEDGMENTS

This work was supported by the US DOE, Office of Basic Energy Sciences, Materials Sciences and Engineering Division (A.N., Q.L., W.G., G.M., A.M., E.D.), by CONICET, Argentina (J.R.), and by the DFG under the Emmy-Noether program (M.D.).

¹For a recent review, see D. C. Johnston, *Adv. Phys.* **59**, 803 (2010), and references therein.

²C. de la Cruz *et al.*, *Nature (London)* **453**, 899 (2008).

³I. I. Mazin, D. J. Singh, M. D. Johannes, and M. H. Du, *Phys. Rev. Lett.* **101**, 057003 (2008).

⁴K. Kuroki, S. Onari, R. Arita, H. Usui, Y. Tanaka, H. Kontani, and H. Aoki, *Phys. Rev. Lett.* **101**, 087004 (2008).

⁵Q. Si and E. Abrahams, *Phys. Rev. Lett.* **101**, 076401 (2008).

⁶A. V. Chubukov, D. V. Efremov, and I. Eremin, *Phys. Rev. B* **78**, 134512 (2008).

- ⁷V. Cvetovic and Z. Tesanovic, *Europhys. Lett.* **85**, 37002 (2009).
- ⁸P. M. R. Brydon and C. Timm, *Phys. Rev. B* **79**, 180504(R) (2009).
- ⁹S. Raghu, X.-L. Qi, C.-X. Liu, D. J. Scalapino, and S.-C. Zhang, *Phys. Rev. B* **77**, 220503 (2008).
- ¹⁰M. Daghofer, A. Moreo, J. A. Riera, E. Arrigoni, D. J. Scalapino, and E. Dagotto, *Phys. Rev. Lett.* **101**, 237004 (2008).
- ¹¹S. Graser, T. A. Maier, P. J. Hirschfeld, and D. J. Scalapino, *New J. Phys.* **11**, 025016 (2009).
- ¹²A. Moreo, M. Daghofer, J. A. Riera, and E. Dagotto, *Phys. Rev. B* **79**, 134502 (2009).
- ¹³A. F. Kemper, T. A. Maier, S. Graser, H.-P. Cheng, P. J. Hirschfeld, and D. J. Scalapino, *New J. Phys.* **12**, 073030 (2010).
- ¹⁴R. Yu, K. T. Trinh, A. Moreo, M. Daghofer, J. A. Riera, S. Haas, and E. Dagotto, *Phys. Rev. B* **79**, 104510 (2009); Q. Luo, G. B. Martins, D.-X. Yao, M. Daghofer, R. Yu, A. Moreo, and E. Dagotto, *ibid.* **82**, 104508 (2010).
- ¹⁵M. Daghofer, A. Nicholson, A. Moreo, and E. Dagotto, *Phys. Rev. B* **81**, 014511 (2010).
- ¹⁶T. Yildirim, *Phys. Rev. Lett.* **101**, 057010 (2008).
- ¹⁷G. S. Uhrig, M. Holt, J. Oitmaa, O. P. Sushkov, and R. R. P. Singh, *Phys. Rev. B* **79**, 092416 (2009).
- ¹⁸F. Krüger, S. Kumar, J. Zaanen, and J. van den Brink, *Phys. Rev. B* **79**, 054504 (2009).
- ¹⁹K. Nakamura, R. Arita, and M. Imada, *J. Phys. Soc. Jpn.* **77**, 093711 (2008).
- ²⁰V. I. Anisimov, D. M. Korotin, M. A. Korotin, A. V. Kozhevnikov, J. Kunes, A. O. Shorikov, S. L. Skornyakov, and S. V. Strelsov, *J. Phys. Condens. Matter* **21**, 075602 (2009).
- ²¹D. H. Lu *et al.*, *Physica C* **469**, 452 (2009).
- ²²J. Zhang, R. Sknepnek, R. M. Fernandes, and J. Schmalian, *Phys. Rev. B* **79**, 220502(R) (2009).
- ²³P. Goswami, P. Nikolic, and Q. Si, *Europhys. Lett.* **91**, 37006 (2010).
- ²⁴K. Seo, B. A. Bernevig, and J. Hu, *Phys. Rev. Lett.* **101**, 206404 (2008).
- ²⁵H. Suhl, B. T. Matthias, and R. L. Walker, *Phys. Rev. Lett.* **3**, 552 (1959).
- ²⁶T. Hotta, *J. Phys. Soc. Jpn.* **79**, 023709 (2010).
- ²⁷L. Boeri, O. V. Dolgov, and A. A. Golubov, *Phys. Rev. Lett.* **101**, 026403 (2008).
- ²⁸T. Shimojima *et al.*, *Science* **332**, 564 (2011).
- ²⁹B. J. Arnold, S. Kasahara, A. I. Coldea, T. Terashima, Y. Matsuda, T. Shibauchi, and A. Carrington, *Phys. Rev. B* **83**, 220504(R) (2011).
- ³⁰Y. Ran, F. Wang, H. Zhai, A. Vishwanath, and D.-H. Lee, *Phys. Rev. B* **79**, 014505 (2009).
- ³¹Y. Wan and Q.-H. Wang, *Europhys. Lett.* **85**, 57007 (2009).
- ³²A. M. Oleś, *Phys. Rev. B* **28**, 327 (1983).
- ³³E. Dagotto, *Rev. Mod. Phys.* **66**, 763 (1994); B. N. Parlett, *The Symmetric Eigenvalue Problem* (Prentice Hall, Upper Saddle River, NJ, 1980).
- ³⁴Qinlong Luo, Dao-Xin Yao, Adriana Moreo, and Elbio Dagotto, *Phys. Rev. B* **83**, 174513 (2011).
- ³⁵P. M. R. Brydon, Maria Daghofer, and Carsten Timm, *J. Phys. Condens. Matter* **23**, 246001 (2011).
- ³⁶Z.-J. Yao, J.-X. Li, Q. Han, and Z. D. Wang, *Europhys. Lett.* **93**, 37009 (2011).
- ³⁷Since the bands are distorted by the interaction term of the Hamiltonian, S_{MB} and S_{TB} do capture the physical properties of the system if the interaction is weak enough so the interacting bands resemble the noninteracting ones.
- ³⁸Ilya Eremin and Andrey V. Chubukov, *Phys. Rev. B* **81**, 024511 (2010).
- ³⁹T. Kariyado and M. Ogata, *J. Phys. Soc. Jpn.* **78**, 043708 (2009).
- ⁴⁰A. Nicholson, W. Ge, X. Zhang, J. A. Riera, M. Daghofer, A. M. Oleś, G. B. Martins, A. Moreo, and E. Dagotto, *Phys. Rev. Lett.* **106**, 217002 (2011).
- ⁴¹R. T. Scalettar, R. R. P. Singh, and S.-C. Zhang, *Phys. Rev. Lett.* **67**, 370 (1991).
- ⁴²J. P. Rodriguez and E. H. Rezayi, *Phys. Rev. Lett.* **103**, 097204 (2009).
- ⁴³F. Cricchio, O. Grånäs, and L. Nordström, e-print arXiv:0911.1342.
- ⁴⁴E. Bascones, M. J. Calderón, and B. Valenzuela, *Phys. Rev. Lett.* **104**, 227201 (2010).